SAND2014-4652C

# Joint Experimental/Computational Investigation Into the Effects of Finite Width on Transonic Cavity Flow

Srinivasan Arunajatesan[*], Matthew F. Barone[†], Justin L. Wagner[‡], Katya M. Casper[§], Steven J. Beresh[**].
*Sandia National Laboratories, Albuquerque, NM, 87185*

**Recently acquired experimental data on pressure fluctuations in cavities of equal length(L) to depth(D) ratio but varying length to width(W) ratio have shown substantial variations in the dominant modes in the cavity. These observations have been carried out at subsonic and transonic Mach numbers at cavity L/D=5, which puts the cavity flow in the "open" category. Classical theory and the current understanding of the flow field dynamics of cavity flows are primarily based on variations with L/D ratio and Mach number and do not explain the observed variation with L/W. A joint computational and experimental investigation has been undertaken at Sandia to explain these observations.**

## I. Introduction

The large fluctuating surface pressure loads observed in aircraft weapons bays represent a serious concern for future military aircraft and stores carried within them. The weapons bay flowfield is very strongly affected by many characteristics such as the flight velocity, the bay geometric features, the presence of stores in the bay, the upstream boundary layer etc[1-3]. Moreover, a wide variety of physical phenomena, e.g. highly unsteady vortex shedding, and strong pressure oscillations characterize this flow. Over the past few decades numerous studies have been aimed at developing a fundamental understanding of the physical mechanisms which drive these fluctuating pressures[4-8]. Unsteady time-accurate computational fluid dynamic simulations of these flow fields have demonstrated the ability to accurately capture these pressure fluctuations[7,8].

Over the past few years a series of experimental and computational investigations has been undertaken at Sandia to characterize, and develop modeling capabilities to capture, the loads experienced by a store in a cavity under captive carriage conditions[9-12]. As part of these investigations, detailed surface pressure measurements, flow field measurements using PIV, and coupled fluid structure interaction modeling have been used to shed light on the processes affecting loads on both the cavity surfaces and the stores inside these cavities.

One of the effects investigated during this effort is that of varying cavity width on the flowfield and surface pressures. These experiments, on supersonic[10] and subsonic cavities[22], have both shown strong changes in the flow field with variations in the Length to Width ratio (L/W) along with changes in the dominant cavity modes (also see Section II for a discussion of these results). Classical theory, such as Rossiter's formula, is based on the physics of longitudinal wave propagation and time scale matching based on the longitudinal dimension of the cavity – these are thus unable to account for effects of the transverse dimension on the flowfield and surface pressures. However, several experimental efforts have cataloged the effect of varying width (or L/W) on cavity pressures and flow field. Early measurements by Block[13] indicated that the dominant effect of width variations was to change the amplitude of the dominant modes – no comments were made in this work regarding the distribution of energy amongst these modes. Experiments by Ahuja and Mendoza[14] suggested that the dominant effect of varying the width of the cavity

[*] Principal Member of the Technical Staff, Engineering Sciences Center, P.O. Box 5800, Mailstop 0825; sarunaj@sandia.gov Senior Member, AIAA.
[†] Principal Member of the Technical Staff, Engineering Sciences Center, Associate Fellow AIAA.
[‡] Senior Member of the Technical Staff, Engineering Sciences Center, AIAA Member.
[§] Senior Member of the Technical Staff, Engineering Sciences Center, AIAA Member.
[**] Distinguished Member of the Technical Staff, Engineering Sciences Center, AIAA Associate Fellow.
This work is supported by Sandia National Laboratories and the United States Department of Energy. Sandia National Laboratories is a multi-program laboratory managed and operated by Sandia Corporation, a wholly owned subsidiary of Lockheed Martin Corporation, for the U.S. Department of Energy's National Nuclear Security Administration under contract DE-AC04-94AL85000

was to change the overall amplitude of the far-field radiated noise. They also were the first to identify the L/W ratio as the dominant parameter governing width effects in cavities. Their measurements (which were restricted to far-field radiated noise) did not show any changes in the distribution of energy amongst the modes. Their experiments were carried out in an open-jet facility, with measurements restricted to far-field noise. The effects of varying width on the cavity wall pressures are difficult to isolate from these measurements. In the work by Tracy and Plentovich[15], measurements under transonic conditions showed that with variations in width for fixed Length to Depth (L/D) ratios, the wall pressure spectra exhibited significant variations in the modal energy distributions along with shifts in the modal frequencies. None of these works however, examined the detailed flowfield in the cavity and its relationship to the surface pressures.

The experiments by Maull and East[16] examined the flow structures in cavities related to the spanwise dimension of the cavity. They identified spanwise cells in the flowfield, the number and distribution of which were related to the dimensions of the cavity (L/D and L/W). However, they did not explain the relationship of these structures to the pressure oscillations in the cavity. Rockwell and Knisely[17] visualized the three-dimensional nature of the flow field using hydrogen bubbles and found secondary streamwise oriented vortices that were spanwise-periodic in the cavity. These structures were seen to disrupt the spanwise vortex structures in the shear layer over the cavity. More recently, Bres and Colonius[18] carried out analysis of three-dimensional instabilities in a cavity flow field and identified the most amplified 3D modes in the flowfield. They found that the frequency of this mode was an order of magnitude lower than the dominant tones in the cavity and that the spanwise dimension of this mode was related to the cavity depth. They correlated this mode to a centrifugal instability of the primary recirculation bubble in the cavity. The properties of these centrifugal instabilities were studied experimentally by Faure et al.[19], at different Reynolds numbers and cavity width to depth aspect ratios. However, these studies too did not relate the flow field information to the surface pressure and the cavity tones.

The recent experiments by Zhang and Naguib[20] focused on the relationship between the flow field and surface pressures and the effects of the spanwise dimension on this relationship. They conducted experiments on an axisymmetric configuration with and without side-walls. However, the pressure oscillation they observed was not of the Rossiter mode type and in fact, was closely matched with the wake mode frequencies observed by Rowley et al[21]. This mode showed strong dependence on the spanwise dimension of the cavity – being absent in wider cavities and strongly amplified in narrower configurations. Their analysis showed that the side walls caused an amplification of the pressure fluctuations on the cavity floor at a distance of about one depth away from the side walls with a similar amplification along the centerline of the cavity for very narrow configurations. Using stochastic estimation, they related this amplification to the penetration of the shear layer vortices into the cavity caused by the three-dimensional flow near the side walls.

The present research is directed at understanding the flow physics of cavities as it potentially relates to vibrational loads that might be induced on stores carried in the cavity. Previous publications from this body of work have shown that the response of structures inside the cavity is a function of both, the loading induced by these pressure fluctuations and the natural structural modes of the store. From this perspective, it is important to understand the cause for the variations in the loading in order to enable a better understanding of the response of stores in the cavity. In this paper, we present analysis of results from numerical simulations of the geometric configurations studied in Wagner et al.[22]. The goal of this work is to shed light on the effects of the spanwise dimension on the cavity flow field and the cavity pressure oscillations.

## II. Background

A detailed account of the experimental observations is presented in Wagner et al.[22], only a brief discussion is presented here to set the context for this work. Experiments were conducted in subsonic and transonic open cavities having a length to depth ratio ( L/D) of 5. Three cavities with dimensions of 5”x5”x1”, 5”x3”x1” and 5”x1”x1” and L/W ratiosof 1.00, 1.67, and 5.00 were tested at three freestream Mach numbers of 0.55, 0.80, and 0.90. In all cases, the boundary layer at the cavity entrance was turbulent with a thickness of about 50% the cavity depth. The data complemented previous supersonic experiments[10] conducted for the same cavity geometries at Mach numbers ranging from 1.5 – 2.5.

Two stereo PIV systems were used simultaneously, to visualize most of the cavity length along the streamwise symmetry plane. Mean velocity data showed the recirculation region to be centered in the cavity for the two wider geometries, whereas the recirculation region shifted downstream for the narrowest cavity (Figure 1). At all Mach numbers, the recirculation region was weakest in the $L/W$ = 1.67 cavity, a trend previously observed at the supersonic Mach numbers.

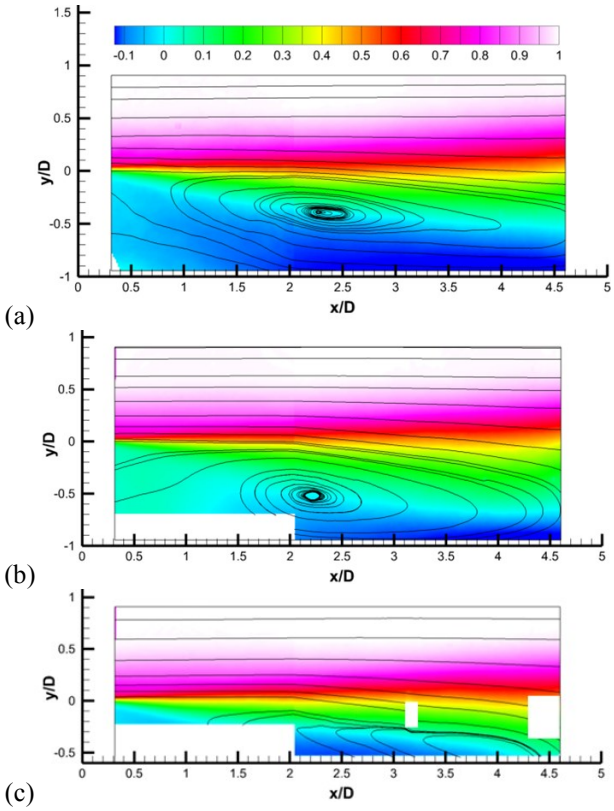


**Figure 1. Mach 0.55 mean streamwise velocity U contours with streamlines superposed at L/W: a) 1.00, b) 1.67, and c) 5.00. The recirculation region moves downstream at the highest L/W. The white rectangles at x/L = 3.2 and 4.5 correspond to masked areas that were corrupted by high background reflections.**

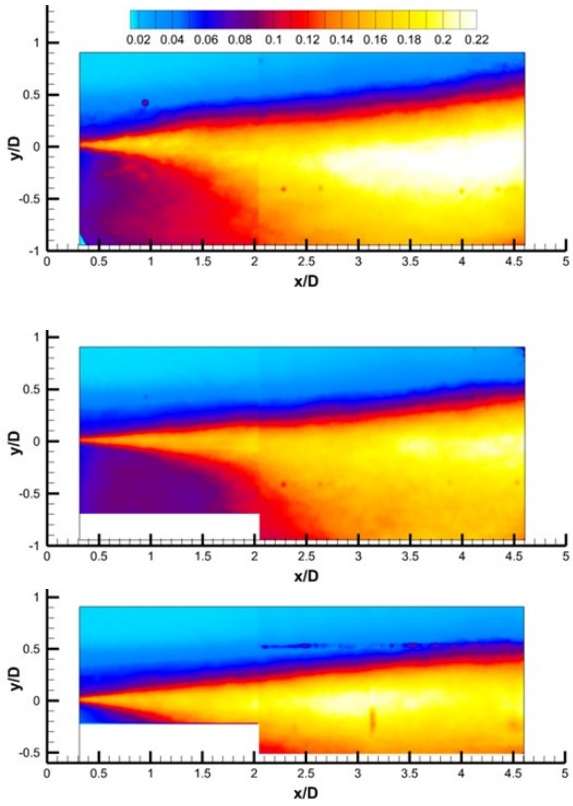


**Figure 2. Mach 0.55 streamwise turbulence intensity contours at L/W: a) 1.00, b) 1.67, and c) 5.00. The data show the turbulence levels to be diminished for the two higher L/W cases.**

As shown in Figure 2 , at Mach = 0.55, the widest cavity(L/W=1.0) exhibits the highest turbulence intensity, with a value of about 0.23. As the aspect ratio is increased the turbulence levels decrease, and for both of the narrower cavities, the peak turbulence intensity is about 0.21. The distribution of turbulence is, however, different for the two narrower cavities. For instance the peak intensity occurs near the aft-wall for the L/W = 1.67 geometry, but near x/L = 3 for L/W = 5.00. This is in contrast to previous supersonic data that showed minimum turbulence levels to occur in the cavity of middle width.

The narrowest cavity exhibited the greatest spanwise coherence at the fore- and aft-walls for all Mach numbers. This observation is possibly related to lower turbulence levels at the walls and/or reduced lateral flow in comparison to the wider cavities, which has been observed at Mach 2.

Wall pressure spectra were computed to investigate potential linkages between trends in the PIV data and the cavity acoustics. The aft-wall centerline SPL spectra are shown for each Mach number and geometry in Figure 3. The Mach 0.55 data show that Rossiter mode 3 is dominant regardless of L/W. In contrast, at Mach 0.8, the mode distribution is different for each L/W. At L/W = 5.00, mode 2 is dominant, but mode 3 also has significant energy. As the cavity widens to L/W = 1.67, mode 1 becomes dominant and peaks are seen at modes 2 – 4, with the magnitude decreasing with mode number. The spectrum for L/W = 1.00 exhibits a dominant mode 2, which is quite different from the other two aspect ratios at this Mach number.

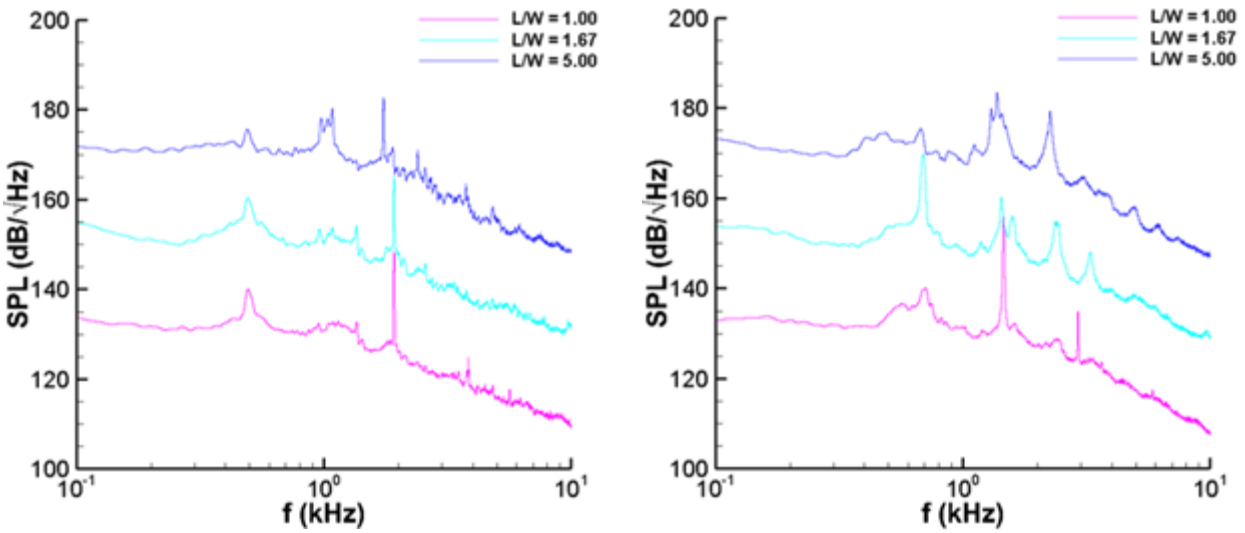


(a). Mach 0.55 (b). Mach 0.80.

**Figure 3. Comparison of cavity aft wall pressure spectra with varying *L*/*W* at subsonic and transonic Mach numbers.**

## III. Computational Methods

The simulations were performed using the SIGMA CFD code, a multi-block, structured grid, finite volume solver for compressible flow. The finite volume method is formally second order, but employs expanded, directionally-split, stencils for constructing the inviscid fluxes, resulting in improved accuracy over standard second order finite volume discretizations. The inviscid flux scheme is a hybrid centered/dissipative scheme, consisting of the sum of a non-dissipative centered flux approximation and a mixed 2nd/5th order dissipative flux that is weighted using a flow sensor to avoid excessive numerical dissipation in regions of resolved turbulent flow (i.e., LES regions). Details of the numerical method can be found in Arunajatesan et al.[12] and Barone and Arunajatesan[23].

The simulations employ a hybrid RANS/LES turbulence model[24], where turbulent flow near the walls is modeled using a k-epsilon RANS model, while further from solid walls the model transitions to LES. The length scale that defines the extent of the near-wall region is set to 0.1 inches for the present simulations. Extensive verification and validation has been carried out on a variety of cavity flows using SIGMA CFD with the present hybrid turbulence model. The validation studies include simulations of various rectangular cavities (empty and containing model stores), and comparison of the results to wind tunnel measurements of wall pressures and velocity flow-fields from several different facilities. The results of these studies have been reported in previous papers[12,23]. In general, the simulation method consistently predicts the frequency of cavity tones to within 5% of measured values, and the amplitude of peaks in the cavity wall pressure spectral density to within 3 dB, with occasional errors in peak amplitude of up to 5 dB.

## IV. Experimental and Simulation Setup

A summary of the relevant wind tunnel campaign studying cavity width effects was given in Section II. These experiments were carried out in Sandia's Tri-sonic Wind Tunnel (TWT). Stereo-PIV data are available within part of the flow-aligned symmetry plane of the cavity. Unsteady wall pressure data on the forward and aft walls of the cavities are also available. Although measurements are available at several Mach numbers, with some observed flow-field variations with Mach number, the present simulation study is focused on the effects of cavity width at a single Mach number of 0.8.

The computational domain spans a large portion of the TWT test section, extending to fifteen inches upstream of the cavity lip to 24 inches downstream of the cavity lip. Velocity and temperature profiles at the inflow boundary, as well as pressure at the outflow boundary, are specified using results from a steady RANS calculation of the flow through the TWT; the domain for the steady calculation extends includes the upstream contraction section and extends the full length of the test section. This approach ensures a proper match of Mach and Reynolds numbers, and that the correct boundary layer profiles are specified for the top and bottom wind tunnel walls (the

cavity is affixed to the top wall). On the side walls, a slip wall boundary condition is applied in order to avoid the computational expense of resolving the side wall boundary layers.

The computational mesh is comprised of 49.4 million volumes divided into two blocks, a cavity block and a tunnel test section block. The dimensions of the cavity block are 250 x 225 x 150 cells in the stream-wise, vertical, and span-wise directions, respectively. This block size was the same for each of the three cavities simulated; thus, the span-wise resolution in the cavity becomes finer and the resolution in the spanwise direction outside the cavity decreases as the cavity width is reduced. Nonetheless, based on previous validation studies, the resolution of the cavity flow-field was deemed adequate for all three cases. A time step of 0.5 microseconds was used for the simulations, and each case was integrated in time for at least 200,000 steps.

The wind tunnel walls were included in the simulations in order to match the experimental conditions as closely as possible. Recent experiments examining the effects of various wall treatments on cavity flow results in the TWT indicate that acoustic interactions with the tunnel walls can have a significant effect on the cavity flow-field, and in particular on the selection of the dominant resonant tones present at a particular free stream Mach number[25]. The body of simulation validation against cavity flow data from the TWT strongly suggest that the present simulation method is capable of capturing these wall effects; however, when interpreting the effects of cavity geometry on the flow within the cavity, the potential presence of wall effects must be kept in mind.

## V. Results and Discussion

The results from the simulations are presented and discussed in this section. First we present comparisons of the simulation results with the measurements in order to establish the quality of the simulation data. These comparisons are limited to the data available from the experiments – wall pressures and mid-span plane PIV measurements of mean and turbulence quantities. Then we examine the simulation results in detail to understand the effects of the varying width on the flow field and the wall pressure signatures.

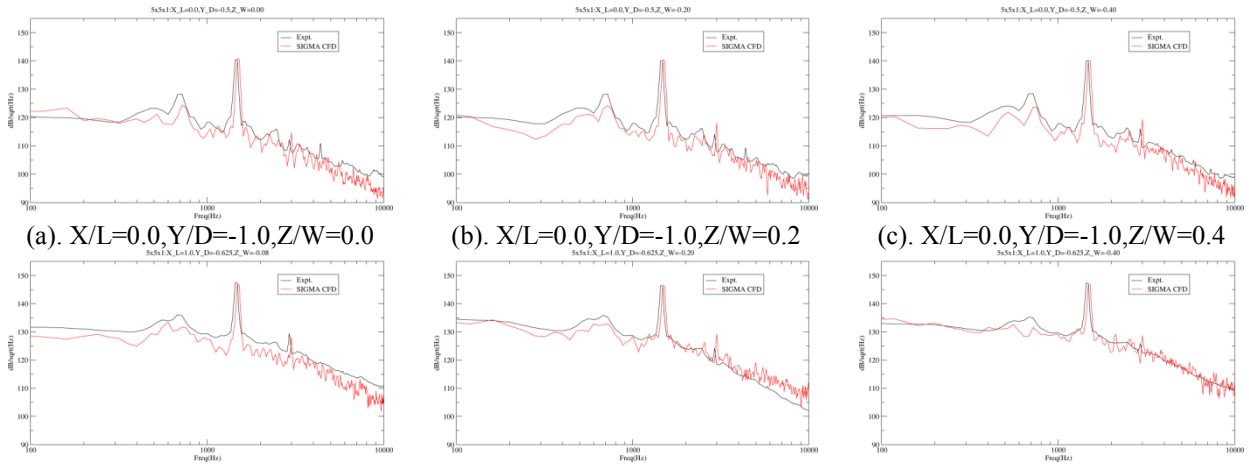


(a). X/L=0.0,Y/D=-1.0,Z/W=0.0 (b). X/L=0.0,Y/D=-1.0,Z/W=0.2 (c). X/L=0.0,Y/D=-1.0,Z/W=0.4

(d). X/L=1.0,Y/D=-1.0,Z/W=0.08 (e). X/L=1.0,Y/D=-1.0,Z/W=0.2 (f). X/L=1.0,Y/D=-1.0,Z/W=0.4

**Figure 4. Comparisons of the aft and front wall pressure spectra for the L/W=1.0 case.**

### A. Wall Pressure Spectra

We first examine comparisons of the wall pressure spectra with experimentally measured spectra. The spectra are computed identically from the experimental and CFD pressure signals using Welch's periodogram method, Hanning windows, 75% overall and a frequency resolution of 40Hz.

Comparisons of the spectra on the aft and fore walls for L/W=1.0 case are shown in Figure 4. The Rossiter modes for this configuration, computed using the modified Rossiter Formula, are shown in Table 1. The spectra show the existence of a single dominant tone corresponding to Rossiter mode 3 with a broad hump in the spectrum corresponding to the mode 2 frequency and a small spike corresponding to mode 5. The comparisons between the simulation results and the measurements are clearly very good –the peak amplitude and frequency of the dominant tone is predicted accurately and the small variations with the location are also captured well by the calculations.

The presence of the single dominant tone is indicative of the presence of interaction of the cavity modes with normal acoustic modes of the tunnel. In the case of the present experimental dataset, it has been observed and documented that this interaction does indeed exist and it does affect the wall pressure spectra measured. The

frequency of the dominant tone (~700 Hz) matches very well the dominant tunnel mode. It is also well understood that in the cases where this interaction exists, it tends to amplify the response at the dominant mode as is the case seen here. From the perspective of the simulations results it is encouraging that these interactions are accurately captured by the simulation method. However, it also emphasizes the need for adequate resolution of the pressure field outside the cavity in order to capture the interaction with the tunnel walls.

**Table 1: Rossiter mode frequencies for the configurations studied here.**

| Mode | Frequency (Hz) |
|---|---|
| 1 | 645.2513 |
| 2 | 1505.586 |
| 3 | 2365.921 |
| 4 | 3226.256 |
| 5 | 4086.591 |
| 6 | 4946.927 |

The results for the L/W=1.67 and and L/W=5.0 case are shown in Figure 5. Here we see that the spectra show a very different characteristic from the L/W=1.0 case with four Rossiter modes – modes 2-5 – clearly seen in the spectra. The predictions are good for the tones at Rossiter modes 3, 4 and 5, but the amplitude of the dominant tone (at mode 2 for L/W=1.67 and mode 3 for L/W=5.0) is under predicted by about 7-8 dB in the calculations. The results are consistent at both the upstream and downstream locations. Again the presence of the dominant second mode tone, and the analysis presented in Wagner et al.[25], suggest the presence of strong interactions between the tunnel modes and the cavity resonant modes. Here, however, we see that the simulation doesn't capture this interaction very well.

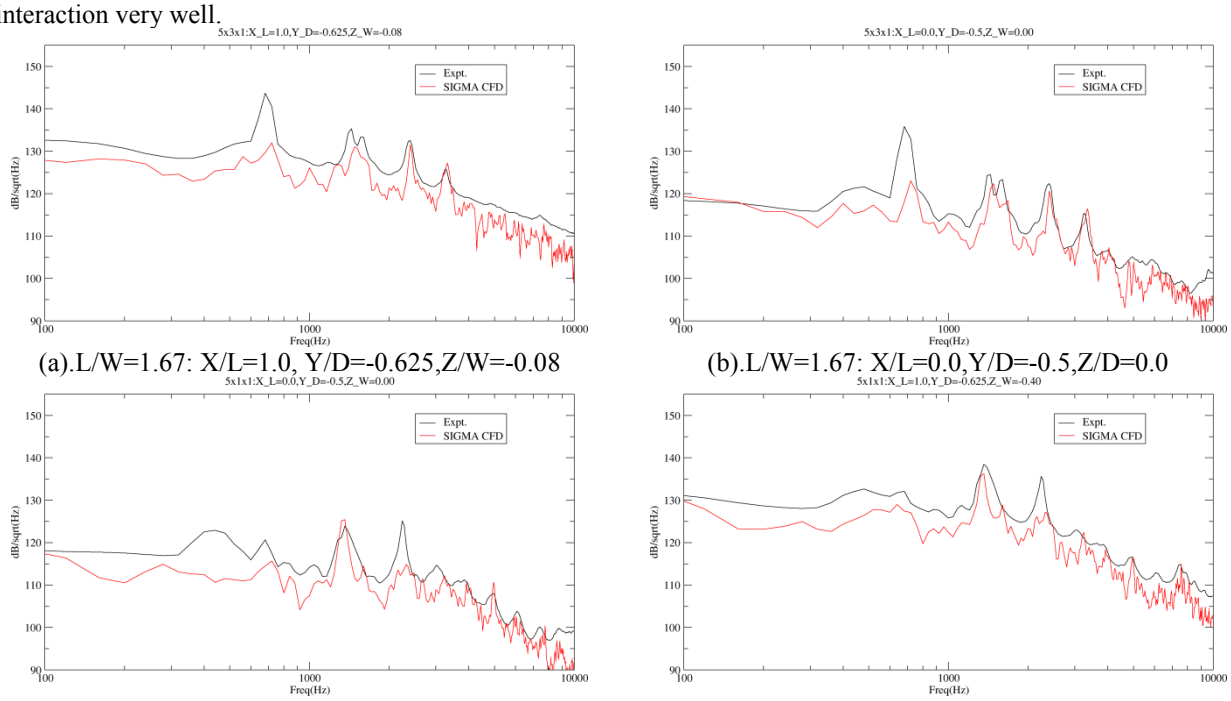


(a).L/W=1.67: X/L=1.0, Y/D=-0.625,Z/W=-0.08

(b).L/W=1.67: X/L=0.0,Y/D=-0.5,Z/D=0.0

(c). L.W=5.0; X/L=0.0,Y/D=0.5,Z/W=0.0

(d). L/W=5.0; X/L=1.0,Y/D=-0.625,Z/W=-0.4

**Figure 5. Wall pressure spectra comparisons for L/W=1.67**

One of the potential reasons for this could be the resolution *outside* the cavity in the simulations. Both the W=5" and W=3" cavity simulations used the same number of grid points across the tunnel and the cavity. In the case of the narrower cavity, a larger domain outside the cavity span was resolved using the same number of points as in the case of the wider cavity, resulting in a poorer resolution in this region outside the cavity. The results presented in Wager et al.[25] suggest that the interaction of the pressure waves with the side walls play a strong role in the tunnel mode

interaction. The poorer resolution in this region for the narrower cavities might be the reason for missing this interaction and under-predicting this modal amplitude.

### B. Flow Field Comparisons

As was mentioned earlier, PIV data was collected on the mid-span plane during the experiments. This data is now compared with the simulation results.

Profiles of the mean streamwise velocity at X/D=1.0, 2.5 and 4.0 for the three cases are compared against measured profiles for the corresponding cases in Figure 6. The experimental uncertainty in the case of the mean velocities in $0.014U_\infty$ - the agreement between the simulations and experiments are well within this range. The profile shapes, the peak negative values in the cavity and the thickness of the shear layer are all predicted well at all the locations for the three cases. It must be noted that due to field of view limitations, the entire depth of the cavity is not visible in the experiments for the narrower cavities.

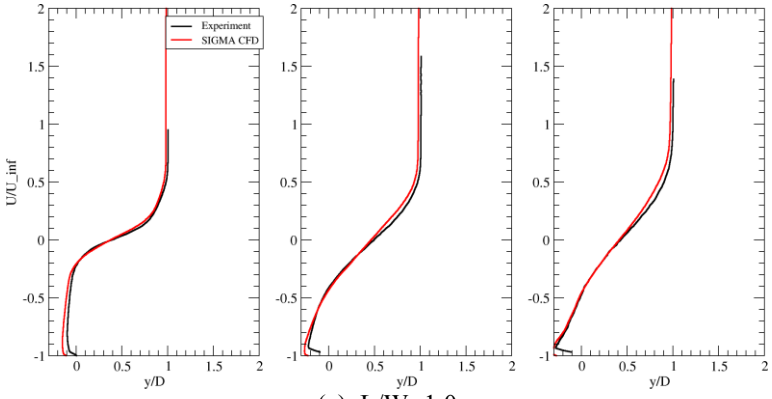


(a). L/W=1.0

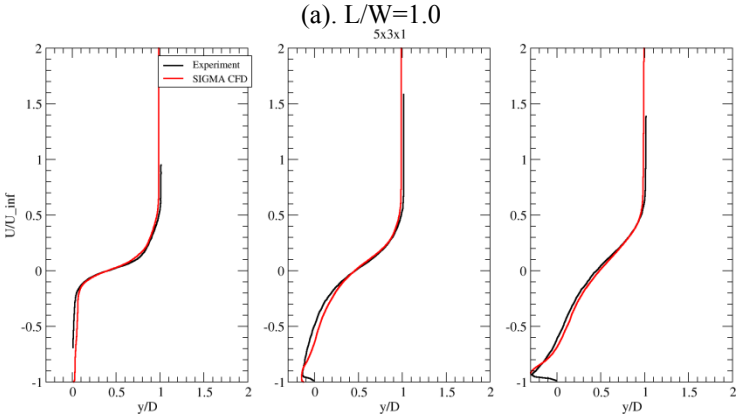


(b). L/W=1.67

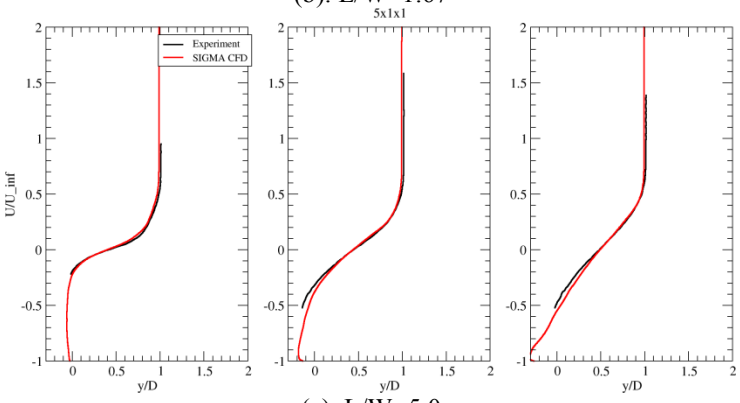


(c). L/W=5.0

**Figure 6.Comparisons of the mean velocity profiles at X/D=1.0,2.5,4.0 (from left to right, respectively) against measured PIV data for the three widths.**

Comparisons of the profiles of the steramwise turbulence intensities at the same three locations are presented in Figure 7. The experimental uncertainties in the turbulence intensities are $0.011U_{\infty}$. At the upstream location (X/L=1.0), the peak intensities are slightly under-predicted , while the location of the peakis predicted fairly well in all three cases. This is probably due to the use of the hybrid RANS-LES model – the tripping of the separating shear layer is potentially delayed bu the use of RANS in the immediate vicinity of the cavity leading edge. At the X/L=2.5 and 4.0 locations, the peak intensities, locations of the peaks and the width of the turbulent region are better predicted. The quality of the agreement between the predicted and measured flow field quantities suggests that the overall mean and turbulent flow fields are well captured by the simulations within the cavity. This further supports the argument presented above that the spanwise resolution of the pressure waves outside the cavity might be responsible for the under-prediction of the modal amplitudes in Figure 4 and Figure 5.

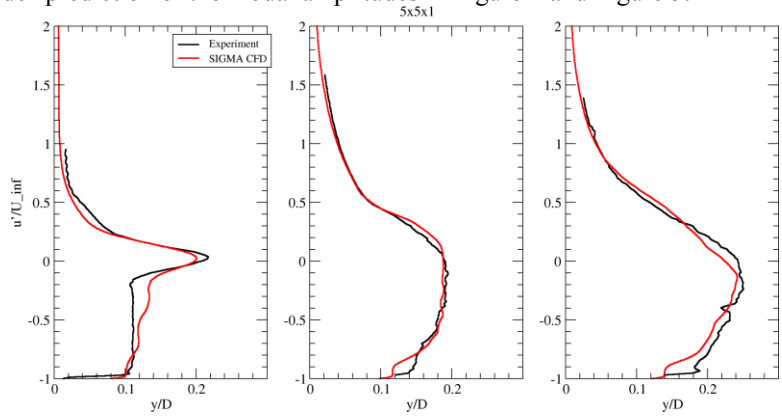


(a). L/W=1.0

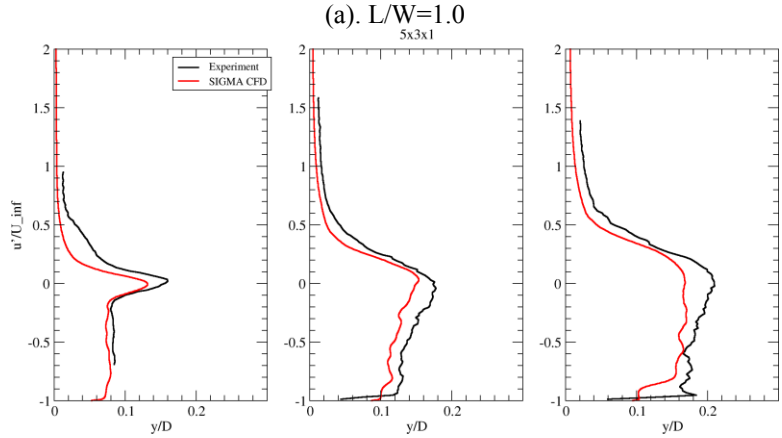


(b). L/W=1.67

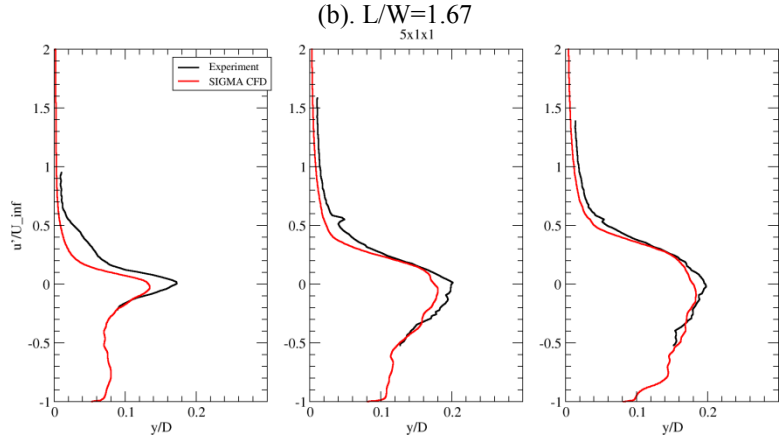


(c). L/W=5.0

**Figure 7. Comparisons of the streamwise turbulence intensity profiles at X/L=1.0,2.5,4.0 (from left to right, respectively) against measured PIV data for the three widths.**

We now further explore the flow field characteristics of the three configurations. In Figure 8, the mean velocity vectors on a plane at X/D=4.75, close to the aftwall is shown. Here, the presence of very strong edge vortices is seen at the side walls of the cavities. In the narrowest cavity, the vectors indicate that the edge vortices are located at the cavity lip-line or slightly below the cavity lipline. In the wider cases, we see that the edge-vortices are located well above the cavity lip-line. In the wider cavities, close to the mid-span section, a clear separation line is visible between the region where the flow turns into the cavity and the region where the flow turns out of the cavity. For the narrowest cavity, however, the flow along the mid-span section is entering the cavity, with the separation line sitting well outside the lip-line of the cavity. The flow entering the cavity just inboard of the edge vortices in the wider cavities is ejected out along the mid-span location. However, in the narrowest cavity the ejection of the fluid out of the cavity is confined to the region very close to the side walls of the cavity.

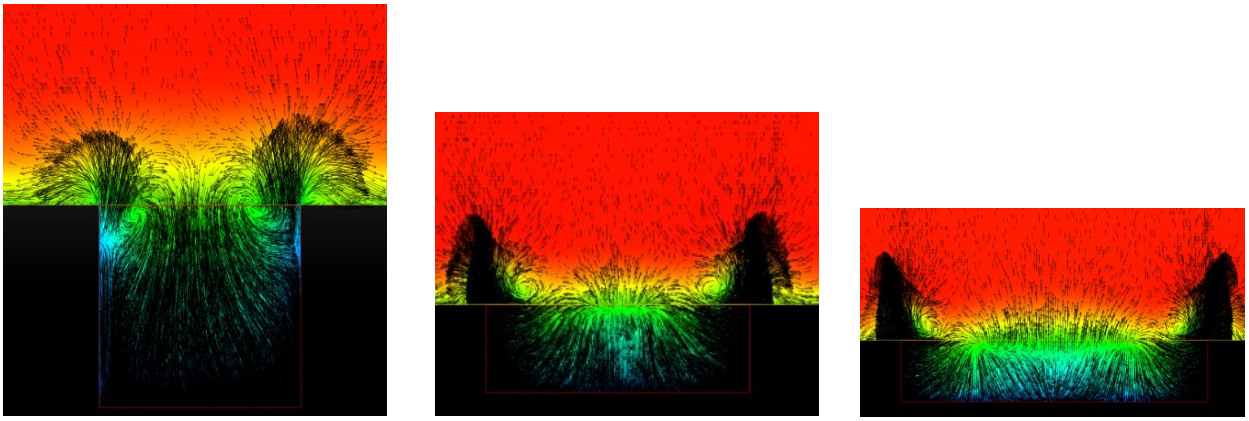

(a)L/W=5.0 (b) L/W=1.67 (c). L/W=1.0

**Figure 8. Mean velocity vectors on constant stream-wise planes at X/D=4.75 for the three cases.**

The streamwise turbulence intensity contours in the cavity, plotted on different spanwise planes are shown in Figure 9. Here, the spanwise planes are located at Z/W=0.0, 0.5 and 0.9 for each of the cases. Certain very distinct characteristics of the flowfields for the three widths are clearly visible in these plots. At the Z/W=0.0 location, the contours for the two narrower cases appear similar with respect to the magnitudes of the intensities and the overall shear layer trajectory. For the widest case, the intensities are significantly higher on this plane and the shear layer trajectory appears to be more "lofted" than for the two narrower cavities. In addition at the upstream half of the cavity, the turbulent region is significantly thicker for this case, than for the two narrower cases. The turbulent region for the widest case appears to grow rapidly to fully encompass the depth of the cavity by X/D = 2.0, while a linearly growing shear layer is visible at this location for the narrower cases. The turbulence intensity in the downstream portion of the cavity is significantly higher for the widest cavity at all the locations.

As we move towards the side-walls of the cavity, this trend in the turbulent region thickness continues, with the widest cavity exhibiting a much thicker turbulent region that the narrower cavities. At the Z/W=0.9 location, we see the effect of the edge vortices on the shear layer – the turbulence intensity for all the three cases increases significantly in this plane. The two wider cases, L/W=1.67 and L/W=1.0 are similar in structure with the L/W=5.0 cavity significantly different from these two. The turbulence intensities for the two wider cases are much higher than for the narrowest case. The shear layer appears to be affected by the edge vortices to a far greater extent in the wide cases than in the narrowest case – the wider the cavity, the more pronounced is the lofting of the shear layer.

Z/W=0.0

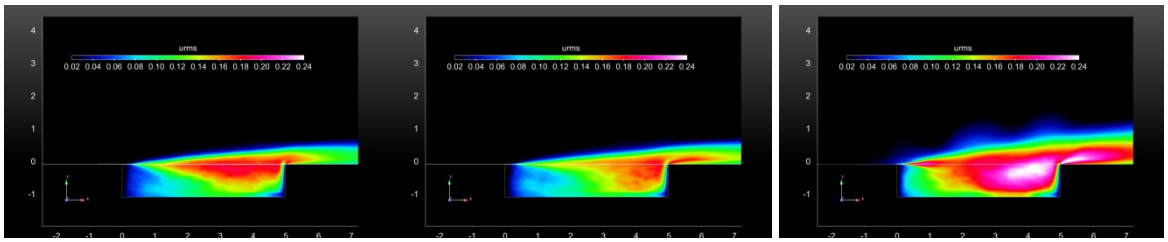

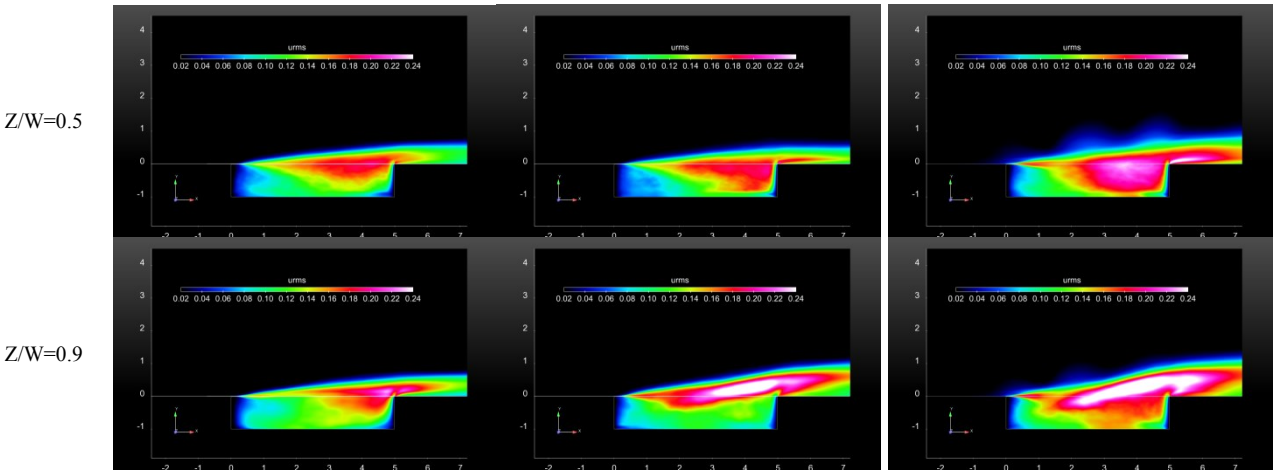


**Figure 9. Streamwise turbulence intensity contours on constant spanwise location planes for L/W=1.0,1.67,5.0.**

This structure is further illustrated by the plots shown in Figure 10. Here, the streamwise turbulence intensity contours are plotted on two streamwise planes at X/D=2.0 and X/D=4.0. In the case of the L/W=5.0 cavity, the turbulent region at the upstream location is confined to the shear layer, with the turbulent region thicker in the middle than close to the cavity side walls. The intensity distribution is fairly uniform across the width of the cavity for this case. In the case of the L/W=1.67 cavity, the turbulent region at the upstream location has a strong spanwise variation. It is very thin in the middle, with low turbulence intensities. The thickness of this region and the turbulence intensity grow towards the cavity walls, where the shear layer interacts very strongly with the edge vortices. For the widest cavity, we see that the turbulent region, even at this location, has more or less completely filled the depth of the cavity. There is a slight increase in the turbulence intensity close to the cavity side walls, where the shear layer interacts with the edge vortices.

At the downstream location the turbulent region has filled the depth of the cavity fully in all three cases. However, there is a strong spanwise variation in the intensity levels for the two wider cases, while the narrowest case again shows a fairly two-dimensional structure. The region of interaction of the shear layer with the edge vortices in the wider cavities sees a very strong increase in the turbulence intensities, indicating stronger fluctuations in the flow field than for the narrowest case.

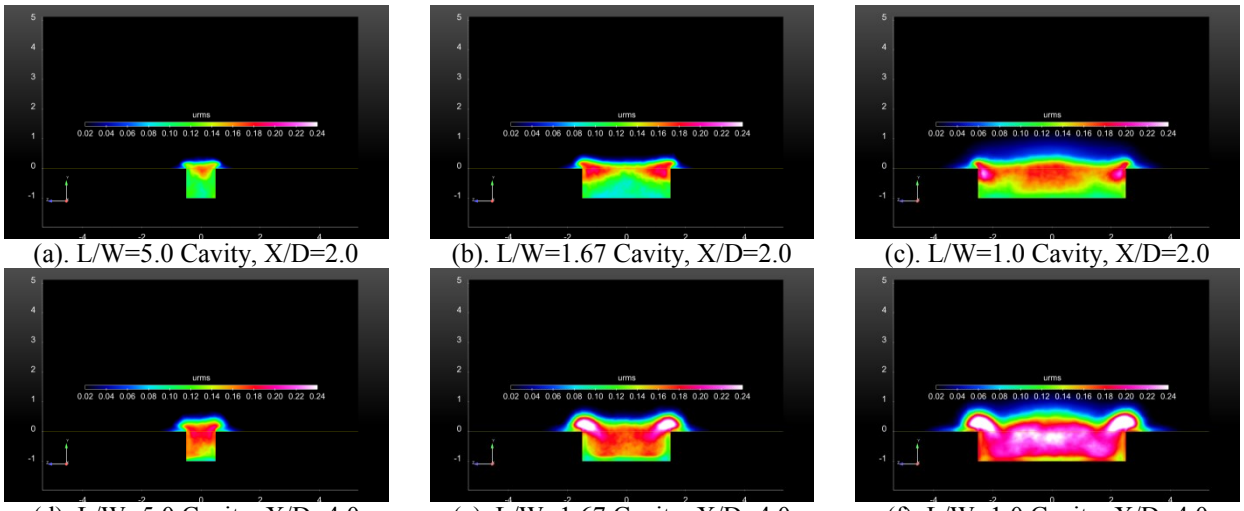

(a). L/W=5.0 Cavity, X/D=2.0 (b). L/W=1.67 Cavity, X/D=2.0 (c). L/W=1.0 Cavity, X/D=2.0

(d). L/W=5.0 Cavity, X/D=4.0 (e). L/W=1.67 Cavity, X/D=4.0 (f). L/W=1.0 Cavity, X/D=4.0

**Figure 10. Streamwise turbulence intensity contours on constant streamwise location planes for L/W=1.0,1.67,5.0.**

The wider turbulent region upstream, the higher turbulence intensities across the cavity and the deeper penetration of the shear layer in the widest cavity case suggests that the shear layer fluctuations are much stronger and more violent in this case than in the two narrower cases. To examine this hypothesis, we look at the cross-correlations of the wall pressures in Figure 11. Here $\phi(\tau) = \overline{p'(r_0,t)p'(r_i,t+\tau)}$ is plotted, where the origin $r_0$ is located at (x/D,y/D) = (5.0,-1.0) and the locations $r_i$ are located at (4.0,-1.0),(3.0,-1.0),(2.0,-1.0),(1.0,-1.0) respectively. The two curves in each graph are correspond to z/D=0.0 and -0.4. From this figure, it is clear that the correlations are extremely strong for the L/W=1.0 case, with a very distinct wave like behavior clearly visible. The magnitude of the correlations remains very high over the entire length of the cavity floor. For the L/W=1.67 and L/W=5.0 cavities, we see a more traditional correlation figure – the correlation has a definite peak time scale with the correlations at larger lags dropping to very low values. The peak correlations for these two cases are of the order of 0.4, while that for the widest cavity is of the order of 0.8. It is interesting, however, that the off-centerline correlations for all the cases are noticeably lower than the centerline correlations at the forward-most location. This is potentially due to the effects of the edge vortices over the cavity sidewalls.

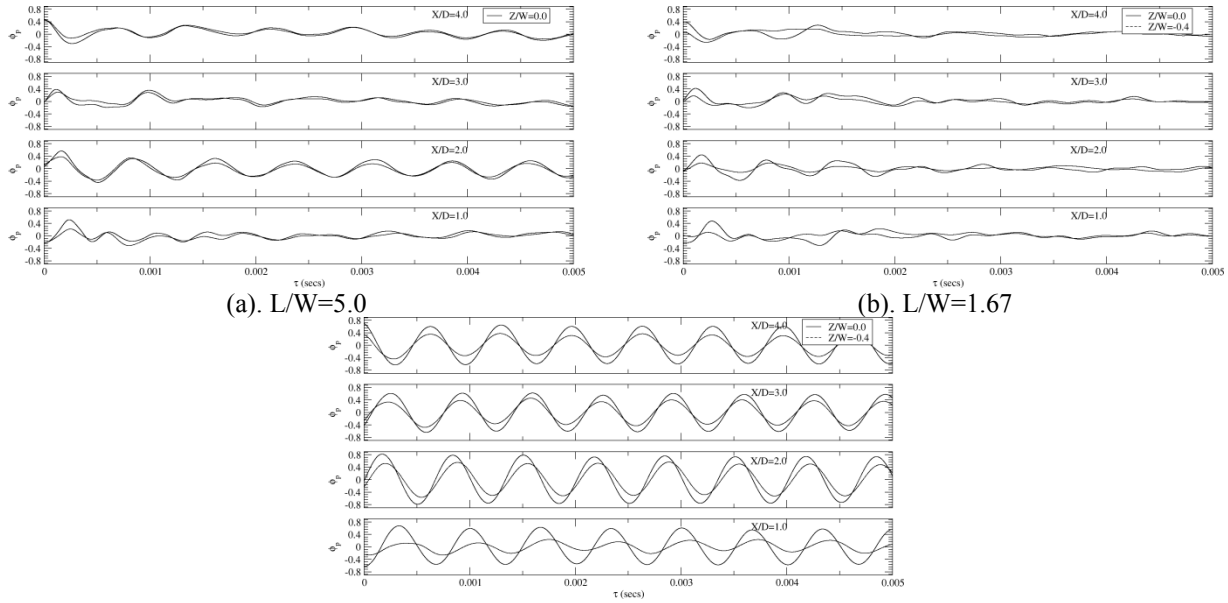


(a). L/W=5.0 (b). L/W=1.67

(c). L/W=1.0

**Figure 11. Cross-correlations of pressure histories on the cavity floor.**

The shear layer behavior is shown in Figure 12 where the cross correlations of the streamwise velocity component along the cavity lip-line are plotted. Here $\phi_u(\tau) = \overline{u'(r_0,t)u'(r_i,t+\tau)}$ are plotted for the three cavities, where the origin $r_0$ is located at (x/D,y/D,z/D) = (0.5,0.0,0.0) and the locations $r_i$ are located at (4.0,0.0,0.0), (3.0,0.0,0.0), (2.0,0.0,0.0), (1.0,0.0,0.0) respectively. Here we see that the shear layer correlations are again much higher for the widest cavity with significantly lower correlations for the L/W=5.0 and 1.67 cavities in comparison. The correlations remain high over the length of the cavity, with a wave like nature indicating large scale coherent oscillations of the shear layer. For the two narrower cases, the oscillations show a distinct peak in the correlation, with decaying correlations for larger times. Based on the correlation times, the shear layer convection velocity for these two cases is calculated to be 0.578 $U_\infty$. For the L/W=1.0 case, this velocity is significantly lower at $0.328U_\infty$.

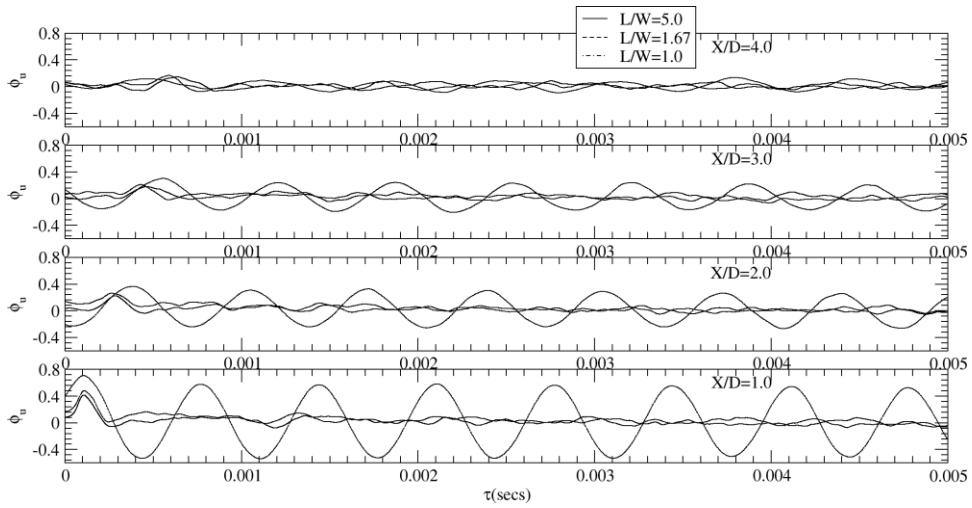


**Figure 12. Cross-correlations of streamwise velocity histories in the shear layer for the three cavities.**

The effect of these large scale shear layer oscillations on the wall pressures are shown in the form of OASPL profiles along the centerline of the cavity floor in Figure 13. For the L/W=1.67 and L/W=5.0 cases, we see that the wall pressure profile has a classical "open" cavity type profile. However, we see that for the widest cavity, the profile has a very different structure. There exists two distinct "nodes" in the profile surrounded by sections of very high amplitude, very similar to what would be seen in a standing wave pattern. This does not resemble a classic open type cavity profile and is clearly dominated by the un-physically large oscillations induced by interactions with the external tunnel walls.

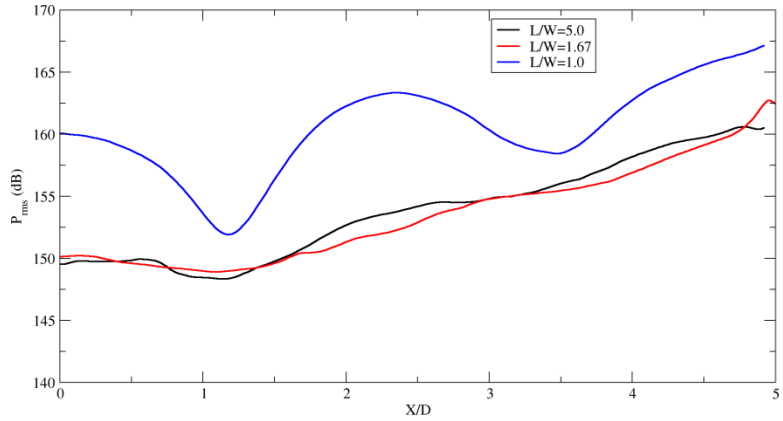


**Figure 13.Wall Pressure OASPL profiles along the floor centerline.**

The shear layer structure is seen in Figure 14 where the contours of density gradient and Mach number are shown for the L/W=1 and L/W=1.67 cavities. The large scale shedding caused by the violent shear layer oscillation is clearly visible for the L/W=1.0 case, while a relatively milder shedding pattern is seen for the L/W=1.67 cavity. Also clearly visible are the strong reflected waves in the tunnel region above the cavity. These are clearly much stronger in the case of the wider cavity due to the strong interactions with the tunnel walls.

## VI. Conclusions and Future Work

The effect of varying L/W on the cavity flow field and wall pressure signatures is explored through the use of experimental data and simulation results of cavities with L/W=1.0,1.67 and 5.0 in a Mach 0.8 flow. The simulation results are able to capture the dominant characteristics seen in the experimental measurement reasonably well. In the case of the widest cavity, the wall pressure spectra are accurately captured, while for the narrower cavities, the amplitude of some of the modes are under-predicted by up to 7dB. Due to solid tunnel walls, existence of interactions of the cavity modes with the tunnel modes is seen and the simulations are able to capture these interactions well. Comparisons of the mean and turbulent flow field shows that the simulation results are in excellent

agreement with the measured values, in most cases within the measurement uncertainty. These results have then been used to examine the effect of the varying widths on the cavity flowfields.

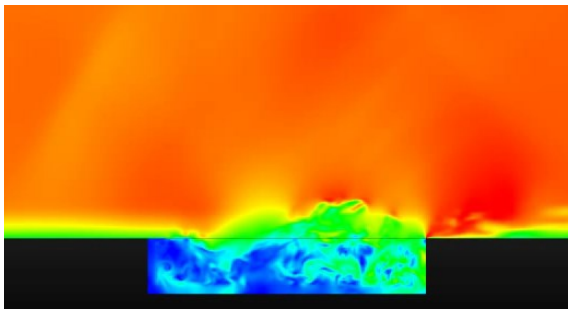

(a). L/W=1.0, Mach Number

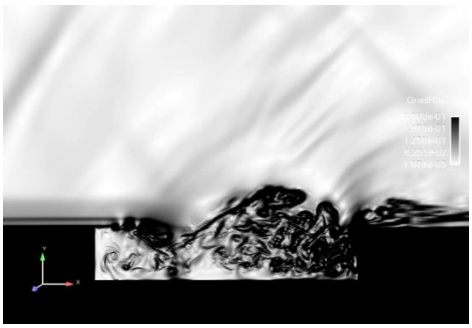

(b). L/W=1.0, Density Gradient

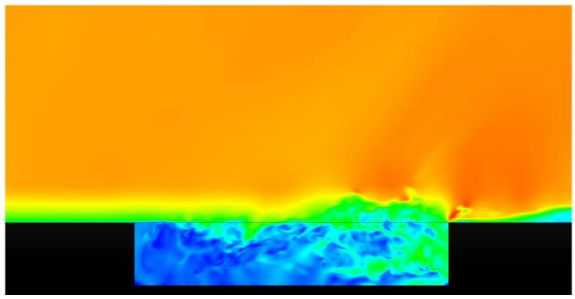

(c). L/W=1.0, Mach Number


(d). L/W=1.67, Density Gradient

**Figure 14. Contour plots of Mach number and Density Gradient for the L/W=1.0 and 1.67 cavities on the mid-span plane.**

The flow-field structures for the three cases are distinctly different. For the widest cavity, the strong coupling with the tunnel modes dominates the flow field, resulting in very strong shear layer oscillations and consequent pressure fluctuations. The wall pressures and shear layer velocities show very strong correlations that persist over the entire length of the cavity. In the case of the narrower cavities, the results show that the L/W=1.67 cavity flow field is strongly affected by the presence of edge vortices along the side walls of the cavity. In the case of the L/W=1.0 cavity, it is too narrow for a similar effect and hence the effect of the edge vortices is noticeable less for this case. The strong shear layer oscillations seen in the widest cavity result in significantly raised turbulence intensity levels everywhere in the cavity, with the turbulent region extending much farther upstream than the other two cases. The L/W=1.67 cavity has much higher turbulence intensities in the vicinity of the side walls than the center line, where the flow is strongly influenced by the edge vortices. In the case of the L/W=5.0 cavity, the spanwise variation in the turbulence intensity is minimal with a near uniform intensities seen across its width.

## References


1. Krishnamurty, K., "Acoustic Radiation from Two-Dimensional Rectangular Cutouts in Aerodynamic Surfaces," NACA, Technical Note 3487, 1955.
2. Rossiter, J., Aeronautical research council reports and memoranda No.3438, 1964
3. Roshko, A., "Some Measurements of Flow in a Rectangular Cutout," NACA, Technical Note 3488, 1955
4. Zhuang, N., Alvi, F.S., Alkislar, M.B., Shih, C., Sahoo, D. and Annaswamy, A.M., "Aeroacoustic Properties of Supersonic Cavity Flows and Their Control", AIAA-2003-3101.
5. Murray, N.E., and Ukeiley, L.S., "Flow Field Dynamics in Open Cavity Flows", AIAA-2006-2428.
6. Arunajatesan, S., Kannepalli, C. and Sinha, N., "Analysis of Control Concepts for Cavity Flows", AIAA Paper 2006-2427, June 2006.
7. Nichols, R.H., "Comparison of Hybrid Turbulence Models for a Circular Cylinder and a Cavity", AIAA Journal, Vol. 44, No. 6, 2006.
8. Arunajatesan, S., Kannepalli, C., Sinha, N., Sheehan, M., Alvi, F. Shumway, G. and Ukeiley, L.S., "Suppression of Cavity Loads Using Leading Edge Blowing", AIAA Journal, Vol. 47, No. 5, 2009.

9. Wagner, J. L., Casper, K. M., Beresh, S. J., Hunter, P. S., Spillers, R. W., Henfling, J. F., Mayes, R. L., "Experimental Investigation of Fluid-Structure Interactions in Compressible Cavity Flows," AIAA Paper 2013-3172.
10. Beresh, S. J., Wagner, J. L., Pruett, B. O., "Supersonic Flow over a Finite-Width Rectangular Cavity," AIAA Paper 2013-0389, Jan. 2013.
11. Arunajatesan, S., Bhardwaj, M., Riley, W. C., and Ross, M., "One-way coupled fluid structure simulations of stores in weapons bays," AIAA Paper 2013-0665, Jan. 2013.
12. Arunajatesan, S., Ross, M., Barone, M., Garret, T. J., "Validation of an FSI Modeling Framework for Internal Captive Carriage Applications," AIAA Paper 2013-2157, June 2013.
13. Block, P.J.W.,"Noise response of cavities of varying dimensionsat subsonic speeds" Technical notes D-8351, National Aeronautics and Space Administration. 1976.
14. Ahuja K.K., Mendoza J., "Effects of cavity dimensions, boundary layer, and temperature on cavity noise with emphasis on benchmark data to validate computational aeroacoustic codes", NASA-CR-4653, 1995.
15. Tracy, M.B., Plentovich, E.B., "Cavity Unsteady-Pressure Measurements at Subsonic and Transonic Speeds", NASA-TM-3669, 1997.
16. Maull, D.J., and East, L.F., "Three Dimensional Flow in Cavities", Journal of Fluid Mechanics, 16:620-632, 1963.
17. Rockwell, D., Knisely, C., "Observations of the 3-D nature of unstable flow past a cavity.", Phys Fluids 23(3):425–431, 1980.
18. Bres, G.A., Colonius, T., "Three-dimensional instability in compressible flow over open cavities", J. Fluid Mech 599:309–339, 2008.
19. Faure, T.M., Pastur, L., Lusseyran, F., Fraigneau, Y., Bisch, D., "Threedimensional centrifugal instabilities development inside a parallelepipedic open cavity of various shape", Exp Fluids 47:395–410, 2009.
20. Zhang, Ke, Naguib, A.M., "Effect of Finite Cavity Width on Flow Oscillation in a low-Mach-number Cavity Flow", Exp. Fluids, 51:1209-1229, 2011.
21. Rowley, C.W., Colonius, T., Basu, A.J., "On self-sustained oscillations in 2-D compressible flow over rectangular cavities", J Fluid Mech 455:315–346, 2002.
22. Wagner, J. L., Beresh, S. J., Casper, K. M., Pruett, B.O., Spillers, R. W., Henfling, "Experimental Investigation of Aspect-Ratio Effects in Transonic and Subsonic Rectangular Cavity Flow," AIAA-2014-1446..
23. Barone, M. and Arunajatesan, S., "Pressure loading within rectangular cavities with and without a captive store", AIAA-2014-1406, 2014.
24. Arunajatesan, S. and Sinha, M., "Hybrid RANS-LES modeling for cavity aeroacoustics predictions", Int. J. Aeronautics, 2(1):65-91, 2003.
25. Wagner, J. L., Casper, K. M., Beresh, S. J., Henfling, J. F., Spillers, R. W., and Pruett, B. O., "Mitigation of wind tunnel wall interactions in subsonic cavity flows", AIAA 2014-XXXX.